Multi-user Ambient Backscatter Communication-Based and STAR-RIS-Aided Mobile Edge Computing Network with Uplink NOMA Scheme: A Joint Design

Dac-Binh Ha[1(✉)], Van-Truong Truong[1], Tien-Vu Truong[2], and Thanh-Minh Phan[3]

[1] Faculty of Electrical-Electronic Engineering, Duy Tan University, Da Nang 550000, Vietnam
hadacbinh@duytan.edu.vn, truongvantruong@dtu.edu.vn

[2] Faculty of Information Technology, Duy Tan University, Da Nang 550000, Vietnam
truongtienvu@dtu.edu.vn

[3] Vietnam Aviation Academy, Ho Chi Minh City, Vietnam
minhpt@vaa.edu.vn

Abstract. This paper presents an ambient backscatter communication (AmBC)-based offloading framework for multi-user non-orthogonal multiple access (NOMA) mobile edge computing (MEC) network. Specifically, in this system multiple resource-constrained mobile users deploy the best user selection and AmBC techniques, as well as the NOMA scheme offloading their tasks to an edge server located at the access point with the help of simultaneous transmitting and reflecting reconfigurable intelligent surface (STAR-RIS). Accordingly, an AmBC-based offloading framework, namely A-STAR, is proposed for this considered system, and a closed-form expression of successful computation probability (SCP) is derived to evaluate the system's latency performance. Numerical results under the Monte-Carlo simulation are provided to verify the correctness of our analysis according to the proposed framework.

Keywords: mobile edge computing · non-orthogonal multiple access · simultaneous transmitting and reflecting reconfigurable intelligent surface · ambient backscatter communication · successful computation probability

1 Introduction

The rapid deployment of real-time applications, such as virtual/augmented reality (VR/AR), unmanned aerial vehicles (UAVs), autonomous driving, and tactile Internet of Things (IoTs), has led to a blooming demand for mobile big data

N.-S. Vo et al. (Eds.): INISCOM 2024, LNICST 595, pp. 93–108, 2024.
https://doi.org/10.1007/978-3-031-67357-3_7

transmitting and computing rates. In order to solve the data transmission problem, there are many techniques applied in previous generations (5G and previous 5G), such as massive multiple-input and multiple-output (MIMO), relaying, selection combining (SC)/maximal ratio combing (MRC), NOMA, backscatter communication, UAV-aided techniques [1–4]. Besides these, some new technical solutions are proposed for the next generation networks (beyond 5G/6G), such as ultra-massive MIMO, intelligent reflecting surface (IRS) or STAR-RIS, millimeter and Terahertz waves, quantum communication, and so on [5]. The combining of these techniques can increase the data transmission and computation rates as well as improve the performance of wireless networks addressing the demand for applications [6]. For example, the work of [7] described the combination of massive MIMO in Terahertz bands; UAV-based MIMO NOMA network was presented in [8]; IRS and NOMA are integrated in [9]; IRS and MIMO with optimization are introduced in [10], and so on.

In our work, we consider the emerging technologies, i.e., ambient backscatter communication (AmBC), STAR-RIS, and NOMA, applied in mobile edge computing (MEC) systems. The MEC technique is a solution to deal with data processing problem by moving the servers to the network's edge for supporting users. Meantime, AmBC is a technique using ambient radio frequency (RF) signals for both energy harvesting and backscattering. This technology allows very low-power communication [11]. Furthermore, the NOMA technique has been introduced recently and is quickly becoming a promising solution to improve spectrum utilization and user capacity by deploying different transmit power levels for each user with the same frequency, time, and code domain [12]. Finally, simultaneous transmitting and reflecting reconfigurable intelligent surfaces (STAR-RIS) can desirably control wireless channels and significantly enhance network performance by leveraging the higher design flexibility and full-space coverage [13]. It is necessary that the integration of these techniques needs to be investigated to evaluate their effectiveness in wireless communication.

1.1 Related Works

In this sub-section, we describe a review of related literature connected to our topic.

According to our knowledge, not many works focus on our related topic. In works [14–16], the integration of STAR-RIS and NOMA in wireless communication networks was studied, in which STAR-RIS is divided into a number of subsurfaces to serve specific multiple users. These results reveal that the combination of STAR-RIS and NOMA can improve the performance of wireless communication networks. Furthermore, the interaction between STAR-RIS and NOMA can enhance the flexibility of network design. A joint architecture of backscattering and uplink NOMA MEC IoT networks was introduced in [17]. In this work, the authors jointly optimized the communication resource of each IoT node and the computation capability of both IoT nodes and the MEC server. The authors in [18] studied the hybrid design of backscattering, RF energy harvesting, and IRS in the MEC network with the time-division multiple access (TDMA)

scheme. They simultaneously maximized system throughput and energy consumption using the Tchebycheff method according to the time/power allocation ratio, local computing frequencies, execution times, backscattering coefficients, and RIS phase shifts. However, the above-mentioned works have not investigated the combination of AmBC, STAR-RIS, and uplink NOMA techniques in multi-user MEC networks.

1.2 Contributions and Organization

Difference with the above literature, in this work, we study a joint design of AmBC, uplink NOMA, and STAR-RIS in a multi-user MEC system with a user selection scheme. In which two users selected from two clusters employ AmBC and deploy the uplink NOMA scheme to offload their tasks to the edge server located at the access point with the assistance of STAR-RIS. The main contributions of our paper are summarized as follows:

- Firstly, we propose a joint design of a multi-user AmBC-based STAR-RIS-aided uplink NOMA MEC system. Accordingly, we also introduce an offloading framework, namely A-STAR, for this proposed system with the best user selection scheme over dissimilar fading channels.
- Secondly, the close-form expression of the successful computation probability (SCP) is derived using the statistical characteristics of new channel power gains.
- Finally, we evaluate SCP with essential system parameters, including average transmit signal-to-noise ratio (SNR), the number of elements of STAR-RIS, and power allocation ratio, to thoroughly comprehend the system's behavior.

Our paper is organized as follows: Sect. 2 presents the system model and communication protocol. The performance analysis is described in Sect. 3. Section 4 provides the numerical results. We conclude our work in Sect. 5.

2 System Model

2.1 System Model and A-STAR Framework Description

Fig. 1 depicts a multi-user AmBC-based STAR-RIS-aided NOMA MEC system model. This system consists of a radio frequency station ($\mathbf{S}$), a cluster of M users with high priority, denoted by $\mathbf{A} = \{A_1, A_2, ..., A_M\}$, a cluster of N users with low priority, denoted by $\mathbf{B} = \{B_1, B_2, ..., B_N\}$, an edge server ($\mathbf{E}$) deployed at the access point (AP), and a STAR-RIS ($\mathbf{R}$) with K_1 elements for fully transmission and K_2 elements for fully reflection located between user clusters and $\mathbf{E}$. Specifically, prior to offloading, a user $A_m \in \mathbf{A}$ $(1 \leq m \leq M)$ and a user $B_n \in \mathbf{B}$ $(1 \leq n \leq N)$ are paired to perform the NOMA scheme for fully offloading by utilizing AmBC. This user-pairing technique is often used in research to ensure the delay in successive interference cancellation (SIC) deployed at AP is significantly reduced [19]. Assuming that STAR-RIS employs K_1 fully

transmission elements to aid A_m, meantime it uses K_2 fully reflection elements to assist B_m offloading their tasks to **E**. All users in **A** and **B** as well as the AP are single-antenna devices, and they operate in half-duplex mode.

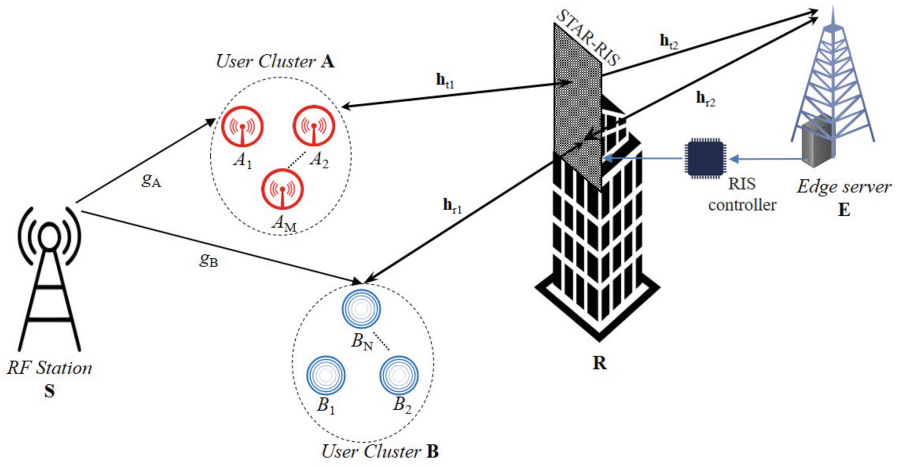

Fig. 1. The proposed STAR-RIS-assisted AmBC-NOMA-MEC system model

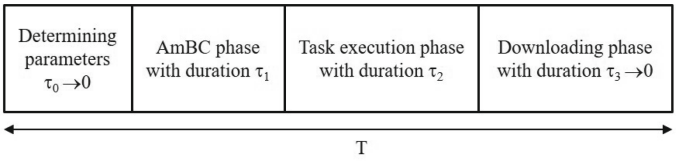

Fig. 2. Time diagram of the A-STAR framework for the proposed system

Based on the proposed system model, we develop an offloading framework that ensures the system's latency requirement, namely A-STAR. Precisely, A-STAR which has time diagram in Fig. 2, consists of 4 phases, described in detail as follows:

- **Parameter determining phase:** In this phase, the channel parameters are estimated. According to the channel state information, a pair of best users $\{A^*, B^*\}$ is selected from **A** and **B**. The controller in Fig. 1 controls the transmission and reflection elements by adjusting their amplitude/phase in real-time. In the scope of our work, we consider the communication between users and AP as well as the task execution at **E**. Therefore, we do not hold this duration in the proposed framework and set $\tau_0 = 0$.
- **AmBC phase:** The user pair $\{A^*, B^*\}$ fully offload their tasks by employing AmBC and applying uplink NOMA scheme under the help of STAR-RIS

during duration τ_1. According to the NOMA scheme, AP employs SIC to decode the required signal. Specifically, **E** decodes the information of A^* first, subtracts it from the received composite signal, and obtains the information of B^* later.

- **Task execution phase:** During this phase, the **E**'s server will execute all the received computation tasks with a duration of τ_2.
- **Downloading phase**: During the last phase, the resultant calculation information will be broadcasted to **A** and **B** by applying downlink NOMA during a duration of τ_3. Following [20,21], τ_3 is significantly short compared to τ_1 and τ_2, hence it is ignored.

2.2 User Selection Scheme

The best users in clusters **A** and **B** are selected for transmission based on the channels from users to the RF station. Given this context, a pair of users in two clusters, **A** and **B**, are selected to maximize the channel power gains of the links from user to **S**. Thus, the selected users in cluster **A** and **B** are respectively given by:

$$A^* = arg \max_{1 \le m \le M} \left\{ |g_{SA_m}|^2 \right\}, \tag{1}$$

$$B^* = arg \max_{1 \le n \le N} \left\{ |g_{SB_n}|^2 \right\}. \tag{2}$$

Accordingly, the channel power gains of this selected links $\{S - A^*, S - B^*\}$ are respectively expressed as

$$X_1 \triangleq g_A = \max_{1 \le m \le M} \left\{ |g_{SA_m}|^2 \right\}, \tag{3}$$

$$X_2 \triangleq g_B = \max_{1 \le n \le N} \left\{ |g_{SB_n}|^2 \right\}. \tag{4}$$

Under Rayleigh fading, the cumulative distribution function (CDF) and probability density function (PDF) of channel power gains g_i ($i \in \{1, 2\}$) are respectively given by

$$F_{X_i}(x) = \left(1 - e^{-\frac{x}{\lambda_0}}\right)^P = \sum_{p=0}^{P} \binom{P}{p} (-1)^p e^{-\frac{px}{\lambda_0}}, \tag{5}$$

$$f_{X_i}(x) = \sum_{p=1}^{P} \binom{P}{p} \frac{(-1)^{p+1} p}{\lambda_0} e^{-\frac{px}{\lambda_0}}, \tag{6}$$

where $P \in \{M, N\}, \lambda_0 = \mathbb{E}[X_i]$. $\mathbb{E}(.)$ stands for the expectation operator.

2.3 STAR-RIS Adjustment

In our proposed system model, the STAR-RIS comprising of K_1 elements for transmission and K_2 elements for reflection operates following to the mode selection protocol [13]. For the sake of simplicity, assume that all STAR-RIS elements transmit and reflect the incoming signals independently. Due to the effect of attenuation, only the signals reflected by the STAR-RIS for the first time are considered, and others will be ignored. Therefore, the signal received from all STAR-RIS elements can be modelled as a combination of their respective transmitted or reflected signals. The small-scale fading vectors of transmission links (A_m-$\mathbf{R}$, $\mathbf{R}-\mathbf{E}$) and reflection links (B_m-$\mathbf{R}$, $\mathbf{R}-\mathbf{E}$) denoted by $\mathbf{h}_{t1} \in \mathbb{C}^{K_1 \times 1}$, $\mathbf{h}_{t2} \in \mathbb{C}^{K_1 \times 1}$, $\mathbf{h}_{r1} \in \mathbb{C}^{K_2 \times 1}$, and $\mathbf{h}_{r2} \in \mathbb{C}^{K_2 \times 1}$, respectively. They are also expressed as

$$\mathbf{h}_{t1} = [h_{t11}, h_{t12}, ..., h_{t1K_1}], \tag{7}$$

$$\mathbf{h}_{t2} = [h_{t21}, h_{t22}, ..., h_{t2K_1}]^T, \tag{8}$$

$$\mathbf{h}_{r1} = [h_{r11}, h_{r12}, ..., h_{r1K_2}], \tag{9}$$

$$\mathbf{h}_{r2} = [h_{r21}, h_{r22}, ..., h_{r2K_2}]^T. \tag{10}$$

The new combination channel coefficients of links from A^* and B^* to $\mathbf{E}$ via STAR-RIS can be expressed as $h_A = \mathbf{h_{t1}}\mathbf{\Phi_1}\mathbf{h_{t2}}$ and $h_B = \mathbf{h_{r1}}\mathbf{\Phi_2}\mathbf{h_{r2}}$, respectively. In which, we define $\mathbf{\Phi_1} \triangleq \text{diag}\left[\alpha_1 e^{j\theta_1}, \alpha_2 e^{j\theta_2}, ..., \alpha_{K_1} e^{j\theta_{K_1}}\right]$ as a diagonal matrix with the amplitude $\alpha_k \in [0,1]$ and phase-shift $\theta_k \in [0, 2\pi)$ are the variables of k^{th} transmitting element of STAR-RIS; meanwhile, $\mathbf{\Phi_2} \triangleq \text{diag}\left[\beta_1 e^{j\phi_1}, \beta_2 e^{j\phi_2}, ..., \beta_{K_2} e^{j\phi_{K_2}}\right]$ is defined as a diagonal matrix with amplitude $\beta_k \in [0,1]$ and phase-shift $\phi_k \in [0, 2\pi)$ are the variables of k^{th} reflecting element of STAR-RIS, $j = \sqrt{-1}$. For simplicity, we assume that $\alpha_k = \alpha$, $\beta_k = \beta$, $\forall k$. Note that, for applying the NOMA scheme, the amplitudes of STAR-RIS elements are adjusted to meet the condition $\alpha > \beta$. Furthermore, in order to assist user's best offloading, the STAR-RIS is reconfigured to the maximum value, i.e., $Y_1 = \max\{|h_A|^2\}$ and $Y_2 = \max\{|h_B|^2\}$, by adjusting the phase-shift variables [22]. Therefore, after deploying the optimal phases θ_k for transmission, the channel power gain of link $A^* - \mathbf{R} - \mathbf{E}$ is given by

$$Y_1 = \left(\alpha \sum_{k=1}^{K_1} |h_{t1k}||h_{t2k}|\right)^2, \tag{11}$$

where $\theta_k = \arg(h_{t1k} h_{t2k})$, $\forall k \in \{1, 2, .., K_1\}$.

Similarly, after deploying the optimal phases ϕ_k for reflection, the channel power gain of link $B^* - \mathbf{R} - \mathbf{E}$ is expressed as

$$Y_2 = \left(\beta \sum_{k=1}^{K_2} |h_{r1k}||h_{r2k}|\right)^2, \tag{12}$$

where $\phi_k = \arg(h_{r1k} h_{r2k})$, $\forall k \in \{1, 2, .., K_2\}$.

According to [22], the CDF and PDF of the random variable $Y_i, i \in \{1, 2\}$ as follows:

$$F_{Y_i}(x) = e^{-\frac{\lambda_i}{2}} \sum_{l=0}^{\infty} \frac{\lambda_i^l \gamma\left(l + \frac{1}{2}, \frac{x}{2K_i(1-\nu_i)\xi}\right)}{l! 2^l \Gamma\left(l + \frac{1}{2}\right)}, \tag{13}$$

$$f_{Y_i}(x) = \sum_{l=0}^{\infty} \frac{e^{-\frac{x}{2K_i(1-\nu_i)\xi} - \frac{\lambda_i}{2}} \lambda_i^l x^{l-\frac{1}{2}}}{l! 2^{2l+\frac{1}{2}} \Gamma\left(l + \frac{1}{2}\right) \left[K_i(1-\nu_i)\xi\right]^{l+\frac{1}{2}}}, \tag{14}$$

where

$$\nu_1 = \frac{1}{m_{t1} m_{t2}} \left[\frac{\Gamma\left(m_{t1} + \frac{1}{2}\right)}{\Gamma\left(m_{t1}\right)}\right]^2 \left[\frac{\Gamma\left(m_{t2} + \frac{1}{2}\right)}{\Gamma\left(m_{t2}\right)}\right]^2, \tag{15}$$

$$\nu_2 = \frac{1}{m_{r1} m_{r2}} \left[\frac{\Gamma\left(m_{r1} + \frac{1}{2}\right)}{\Gamma\left(m_{r1}\right)}\right]^2 \left[\frac{\Gamma\left(m_{r2} + \frac{1}{2}\right)}{\Gamma\left(m_{r2}\right)}\right]^2, \tag{16}$$

$\xi \in \{\alpha^2, \beta^2\}$, $\lambda_i = \frac{K_i \nu_i}{1-\nu_i}$ and $\gamma(.,.)$ is the lower incomplete gamma function.

2.4 New Channel Statistics

By applying AmBC, we form the integrated channel power gains of triple-hop links $\mathbf{S} - A^* - \mathbf{R} - \mathbf{E}$ and $\mathbf{S} - B^* - \mathbf{R} - \mathbf{E}$ as follows:

$$Z_1 = X_1 Y_1 = g_A \left(\alpha \sum_{k=1}^{K_1} |h_{t1k}||h_{t2k}|\right)^2, \tag{17}$$

$$Z_2 = X_2 Y_2 = g_B \left(\beta \sum_{k=1}^{K_2} |h_{r1k}||h_{r2k}|\right)^2. \tag{18}$$

During AmBC phase, $\mathbf{E}$ employs SIC to decode the signal from A^*, x_{A^*}, first by treating the signal from B^*, x_{B^*}, as a noise. Thus, the signal-to-interference-plus-noise ratio (SINR) to detect x_{A^*} at $\mathbf{E}$ is given by

$$\gamma_A = \frac{\gamma_0 Z_1}{\gamma_0 Z_2 + 1}, \tag{19}$$

where $\gamma_0 \triangleq \frac{P_S}{\sigma^2}$ is the average transmit SNR of $\mathbf{S}$, P_S is the transmit power of $\mathbf{S}$.

The signal-to-noise ratio (SNR) at $\mathbf{E}$ after subtracting x_{A^*} from the received superimposed signal to detect x_{B^*} is written as

$$\gamma_B = \gamma_0 Z_2. \tag{20}$$

New channel statistics for the power gains (Z_1 and Z_2) can be obtained by the following Lemma:

Lemma 1. *The CDF and PDF of variable* $Z_i (i \in \{1, 2\})$ *defined as (17) and (18) can be written as*

$$F_{Z_i}(x) = 1 + e^{-\frac{\lambda_i}{2}} \sum_{p=1}^{P} \sum_{q=0}^{\infty} \binom{P}{p} \frac{(-1)^p \lambda_i^q}{q! 2^{(2q-\frac{1}{2})} \Gamma\left(q + \frac{1}{2}\right))} \times \left(\sqrt{\frac{2px}{\lambda_0 K_i (1-\nu_i)\xi}} \right)^{q+\frac{1}{2}} \mathcal{K}_{q+\frac{1}{2}} \left(\sqrt{\frac{2px}{\lambda_0 K_i (1-\nu_i)\xi}} \right), \quad (21)$$

$$f_{Z_i}(x) = e^{-\frac{\lambda_i}{2}} \sum_{p=1}^{P} \sum_{q=0}^{\infty} \binom{P}{p} \frac{(-1)^{p+1} \lambda_i^q}{q! 2^{(2q+\frac{1}{2})} \Gamma\left(q + \frac{1}{2}\right))} \times \frac{1}{x} \left(\sqrt{\frac{2px}{\lambda_0 K_i (1-\nu_i)\xi}} \right)^{q+\frac{3}{2}} \mathcal{K}_{q-\frac{1}{2}} \left(\sqrt{\frac{2px}{\lambda_0 K_i (1-\nu_i)\xi}} \right), \quad (22)$$

where $P \in \{M, N\}$, $\mathcal{K}_\nu(.)$ *denotes the modified Bessel function of the second kind of* ν^{th}*-order.*

Proof. See Appendix A.

3 Performance Analysis

The successful computation probability (SCP) is an important metric to evaluate the latency performance of MEC systems [23]. In this section, we present the derivation of closed-form expression of SCP. This metric is defined as the probability that system latency is lower than the maximum allowed time, i.e.,

$$SCP = \Pr\left(\tau_1 + \tau_2 < T\right), \quad (23)$$

where

$$\tau_1 = \max\left\{\frac{L_A}{C_A}, \frac{L_B}{C_B}\right\}, \quad (24)$$

$$\tau_2 = \frac{cL}{f}, \quad (25)$$

$C_A = W\log_2(1+\gamma_A)$, $C_B = W\log_2(1+\gamma_B)$, $L = L_A + L_B$, c and f denote the number of CPU cycles needed for executing each bit and the CPU-cycle frequency of the MEC server at **E**, respectively, and W denotes the channel bandwidth. Thus, we state **Theorem** 1 describing the SCP expression as follows:

Theorem 1. *The SCP of the proposed AmBC-based STAR-RIS-aided NOMA MEC system operating under the A-STAR framework is given by:*

$$SCP = \begin{cases} 0, & if \quad T-\tau_2 \le 0, \\ \frac{\pi e^{-\frac{\lambda_1+\lambda_2}{2}}}{Q} \sum_{p_1=1}^{M} \sum_{p_2=1}^{N} \sum_{q_1=0}^{\infty} \sum_{q_2=0}^{\infty} \sum_{q=1}^{Q} \binom{M}{p_1} \binom{N}{p_2} \\ \frac{(-1)^{p_1+p_2} \lambda_1^{q_1} \lambda_2^{q_2}}{q_1! q_2! 2^{2(q_1+q_2)} \Gamma\left(q_1+\frac{1}{2}\right) \Gamma\left(q_2+\frac{1}{2}\right) z_q} \sqrt{\frac{1-\omega_q}{1+\omega_q}} \\ \left(\frac{1}{\alpha}\sqrt{\frac{2p_1 \Lambda_A(\gamma_0 z_q+1)}{\lambda_0 K_1(1-\nu_1)\gamma_0}}\right)^{q_1+\frac{1}{2}} \left(\frac{1}{\beta}\sqrt{\frac{2p_2 z_q}{\lambda_0 K_2(1-\nu_2)}}\right)^{q_2+\frac{3}{2}} \\ \mathcal{K}_{q_1+\frac{1}{2}}\left(\frac{1}{\alpha}\sqrt{\frac{2p_1 \Lambda_A(\gamma_0 z_q+1)}{\lambda_0 K_1(1-\nu_1)\gamma_0}}\right) \mathcal{K}_{q_2-\frac{1}{2}}\left(\frac{1}{\beta}\sqrt{\frac{2p_2 z_q}{\lambda_0 K_2(1-\nu_2)}}\right), & if \quad T-\tau_2 > 0, \end{cases} \tag{26}$$

where $\Lambda_A = 2^{\frac{L_A}{W(T-\tau_2)}} - 1$, $\Lambda_B = 2^{\frac{L_B}{W(T-\tau_2)}} - 1$, $z_q = -\ln\frac{(\omega_q+1)a}{2}$, $a = \exp\left(-\frac{\Lambda_B}{\gamma_0}\right)$, $\omega_q = \cos\left(\frac{2q-1}{2Q}\pi\right)$, *and* Q *is the complexity-vs-accuracy trade-off coefficient.*

Proof. See Appendix B.

4 Numerical Results and Discussion

This section provides the numerical results regarding the SCP of AmBC-based STAR-RIS-aided NOMA MEC system. Monte-Carlo simulations are employed to confirm the analytical results. Similar to the work of [24], we provide the typical values of simulation parameters utilized in our work as Table 1.

Figure 3 draws the curve of SCP versus the average transmit SNR with different numbers of STAR-RIS's elements. From this figure, we can observe that SCP upgrades when γ_0 and/or K_1 and/or K_2 increase. It means that the performance of this considered system can be improved by increasing the transmit power and/or the number of STAR-RIS's elements. In other words, STAR-RIS can effectively assisted NOMA users to offload their tasks to MEC servers.

Figures 4 and 5 depicts the impact of the number of users in clusters **A** and **B**. From these figures, we can see that SCP increases when M and/or N increase. It means that the increasing of number of users allows we choose the better user to offload its task to AP. However, the increasing of the number of high-priority users improves the performance less than comparing to the increasing of the number of low-priority users.

Figure 6 illustrates the effect of the power allocation ratio ξ on the SCP of our considered system with different average transmit SNR values. Note that the variation of $\xi \in \{\alpha^2, \beta^2\}$ can be obtained by adjusting the amplitudes of each STAR-RIS's element. This adjustment can meet the condition of successive interference cancellation when the paired users have similar channel gains. We can observe from this figure that the system can reach to the best performance in the middle range of ξ value. In other words, there exists a pair of optimal

Table 1. Simulation Parameters

Parameters	Notation	Typical Values
Environment		Rayleigh, Nakagami-m
Rayleigh fading parameter	λ_0	1
Nakagami-m parameters for transmission	m_{t1}, m_{t2}	3, 3
Nakagami-m parameters for reflection	m_{r1}, m_{r2}	2, 2
The number of transmission elements	K_1	6
The number of reflection elements	K_2	4
Transmission amplitude	α^2	0.75
Reflection amplitude	β^2	0.25
The average transmit SNR	γ_0	0 - 30 dBm
The CPU-cycle frequency of MEC server	f	1 GHz
The number of CPU cycles for computing each bit at MEC server	c	2
Channel bandwidth	W	500 MHz
The length of task A, task B	$\{L_A, L_B\}$	{0.6, 0.4} Mbits
The threshold of latency	T	20 ms
Number of points for Gaussian-Chebyshev quadrature method	Q	50

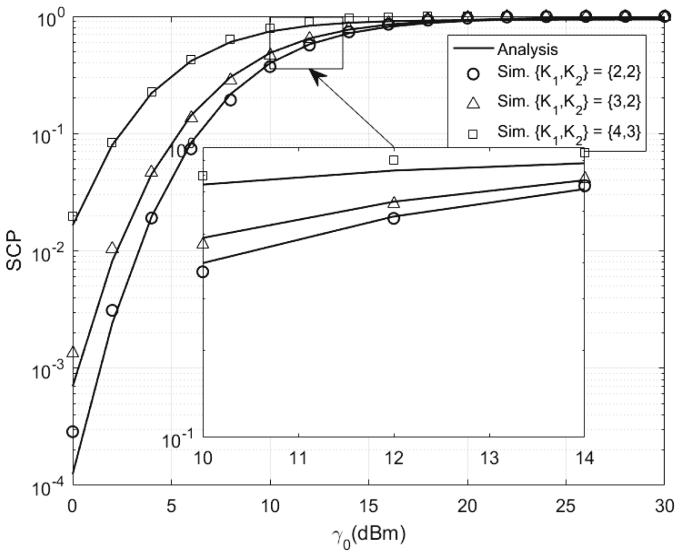

Fig. 3. SCP vs. the average transmit SNR γ_0 with different number of STAR-RIS's elements

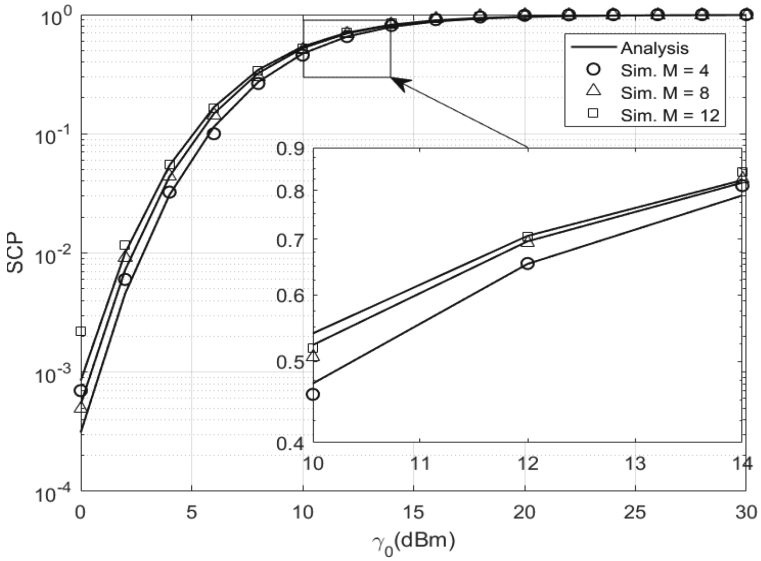

Fig. 4. SCP vs. γ_0 with different number of users in **A**

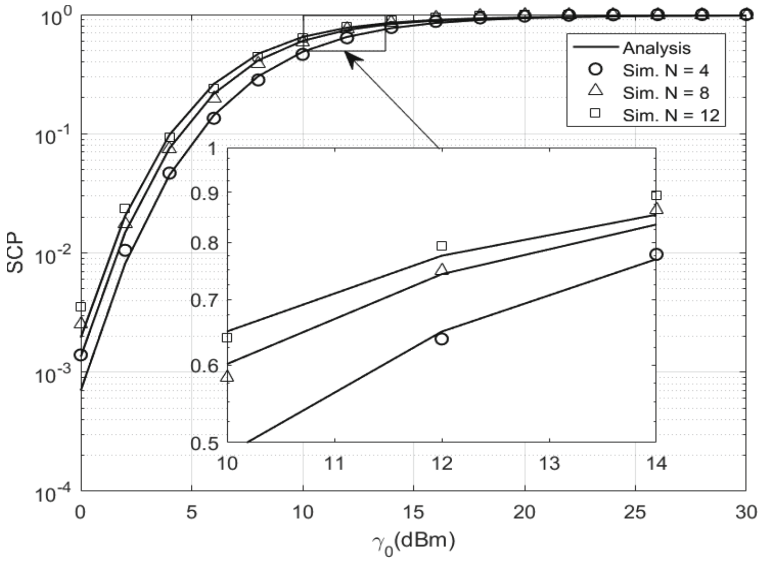

Fig. 5. SCP vs. γ_0 with different number of users in **B**

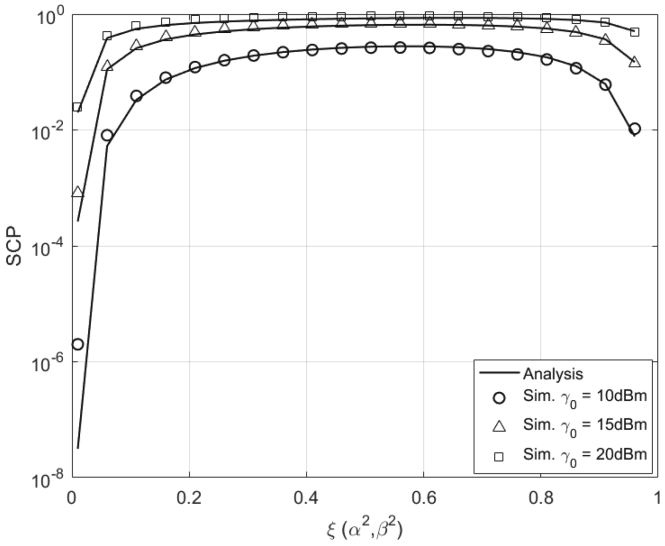

Fig. 6. SCP vs. power allocation ratio with different average transmit SNR values

values $\{\alpha^*, \beta^*\}$ that we can adjust the STAR-RIS's amplitudes to make SCP achieving the highest point.

Figure 3, 4, 5 and 6 show that the simulated values match the computational theory. That proved the correctness of our analysis.

5 Conclusion

In this paper, we have proposed a joint design for MEC network in which the combination of AmBC, STAR-RIS, uplink NOMA, and user selection schemes is applied. Accordingly, a new offloading A-STAR framework is introduced, and the expression of successful computation probability is derived by utilizing the statistical characteristics of multi-hop channels. Finally, the impacts of system key parameters on this considered network's performance were investigated to reveal that the increasing of the number of users and/or the number of STAR-RIS's elements and/or transmit power can enhance the latency performance. In our future work, we will consider the optimization problem of this proposed system.

Acknowledgment. This research is funded by Vietnam National Foundation for Science and Technology Development (NAFOSTED) under grant number 102.04–2021.11.

APPENDIX A: PROOF OF LEMMA 1

The CDF of variable $Z_i (i \in \{1,2\})$ can be expressed as

$$F_{Z_i}(x) = \Pr\left(Z_i < x\right) = \Pr\left(X_i Y_i < x\right) = \int_0^{\infty} F_{X_i}\left(\frac{x}{y}\right) f_{Y_i}(y) dy \tag{A-1}$$

By substituting (5) and (14) into the integral in (A-1), after some manipulations and employing the equation (3.471.9) in [25], we obtain

$$\begin{aligned} F_{Z_i}(x) = 1 + e^{-\frac{\lambda_i}{2}} \sum_{p=1}^{P} \sum_{q=0}^{\infty} \binom{P}{p} \frac{(-1)^p \lambda_i^q}{q! 2^{(2q-\frac{1}{2})} \Gamma\left(q+\frac{1}{2}\right))} \\ \times \left(\sqrt{\frac{2px}{\lambda_0 K_i (1-\nu_i)\xi}}\right)^{q+\frac{1}{2}} \mathcal{K}_{q+\frac{1}{2}}\left(\sqrt{\frac{2px}{\lambda_0 K_i (1-\nu_i)\xi}}\right). \end{aligned} \tag{A-2}$$

Next, we derivative (A-2) by applying the result of (8.486–14) in [25] to get the PDF as follows:

$$\begin{aligned} f_{Z_i}(x) = e^{-\frac{\lambda_i}{2}} \sum_{p=1}^{P} \sum_{q=0}^{\infty} \binom{P}{p} \frac{(-1)^{p+1} \lambda_i^q}{q! 2^{(2q+\frac{1}{2})} \Gamma\left(q+\frac{1}{2}\right))} \\ \times \frac{1}{x} \left(\sqrt{\frac{2px}{\lambda_0 K_i (1-\nu_i)\xi}}\right)^{q+\frac{3}{2}} \mathcal{K}_{q-\frac{1}{2}}\left(\sqrt{\frac{2px}{\lambda_0 K_i (1-\nu_i)\xi}}\right). \end{aligned} \tag{A-3}$$

This concludes our proof.

APPENDIX B: PROOF OF THEOREM 1

Based on the definition formula, SCP can be rewritten as follows:

$$\begin{aligned} SCP &= \Pr\left(\frac{L_A}{W \log_2\left(1+\gamma_A\right)} < T-\tau_2, \frac{L_B}{W \log_2\left(1+\gamma_B\right)} < T-\tau_2\right) \\ &= \begin{cases} 0, & if \quad T-\tau_2 \le 0 \\ \Pr\left(\frac{\gamma_0 Z_1}{\gamma_0 Z_2+1} > \Lambda_A, \gamma_0 Z_2 > \Lambda_B\right), & if \quad T-\tau_2 > 0 \end{cases} \\ &= \begin{cases} 0, & if \quad T-\tau_2 \le 0 \\ \Pr\left(Z_1 > \frac{\Lambda_A}{\gamma_0}(\gamma_0 Z_2+1), Z_2 > \frac{\Lambda_B}{\gamma_0}\right), & if \quad T-\tau_2 > 0 \end{cases} \\ &= \begin{cases} 0, & if \quad T-\tau_2 \le 0 \\ 1 - F_{Z_2}\left(\frac{\Lambda_B}{\gamma_0}\right) - \underbrace{\int_{\frac{\Lambda_B}{\gamma_0}}^{\infty} F_{Z_1}\left(\frac{\Lambda_A(\gamma_0 z+1)}{\gamma_0}\right) f_{Z_2}(z) dz}_{I}, & if \quad T-\tau_2 > 0 \end{cases}. \end{aligned} \tag{B-1}$$

where $\Lambda_A = 2^{\frac{L_A}{W(T-\tau_2)}} - 1$, $\Lambda_B = 2^{\frac{L_B}{W(T-\tau_2)}} - 1$.

By substituting (A-2) and (A-3) into (B-1), the integral I can be rewritten as

$$\begin{aligned} I = 1 - F_{Z_2}(\frac{\Lambda_B}{\gamma_0}) - \sum_{p_1=1}^{M}\sum_{p_2=1}^{N}\sum_{q_1=0}^{\infty}\sum_{q_2=0}^{\infty}\binom{M}{p_1}\binom{N}{p_2} \\ \frac{(-1)^{p_1+p_2}\lambda_1^{q_1}\lambda_2^{q_2}e^{-\frac{\lambda_1+\lambda_2}{2}}}{q_1!q_2!2^{(2q_1+2q_2)}\Gamma\left(q_1+\frac{1}{2}\right))\Gamma\left(q_2+\frac{1}{2}\right))} \\ \int_{\frac{\Lambda_B}{\gamma_0}}^{\infty}\left(\frac{1}{\alpha}\sqrt{\frac{2p_1\Lambda_A(\gamma_0 z+1)}{\lambda_0 K_1(1-\nu_1)\gamma_0}}\right)^{q_1+\frac{1}{2}}\mathcal{K}_{q_1+\frac{1}{2}}\left(\frac{1}{\alpha}\sqrt{\frac{2p_1\Lambda_A(\gamma_0 z+1)}{\lambda_0 K_1(1-\nu_1)\gamma_0}}\right) \\ \left(\frac{1}{\beta}\sqrt{\frac{2p_2 z}{\lambda_0 K_2(1-\nu_2)}}\right)^{q_2+\frac{3}{2}}\mathcal{K}_{q_2-\frac{1}{2}}\left(\frac{1}{\beta}\sqrt{\frac{2p_2 z}{\lambda_0 K_2(1-\nu_2)}}\right)\frac{dz}{z}. \end{aligned} \tag{B-2}$$

By setting $t = e^{-z}$ and applying the Gaussian-Chebyshev quadrature method to calculate the integral, we obtain the following result:

$$\begin{aligned} I = 1 - F_{Z_2}(\frac{\Lambda_B}{\gamma_0}) - \frac{\pi e^{-\frac{\lambda_1+\lambda_2}{2}}}{Q}\sum_{p_1=1}^{M}\sum_{p_2=1}^{N}\sum_{q_1=0}^{\infty}\sum_{q_2=0}^{\infty}\sum_{q=1}^{Q}\binom{M}{p_1}\binom{N}{p_2} \\ \frac{(-1)^{p_1+p_2}\lambda_1^{q_1}\lambda_2^{q_2}}{q_1!q_2!2^{(2q_1+2q_2)}\Gamma\left(q_1+\frac{1}{2}\right)\Gamma\left(q_2+\frac{1}{2}\right)z_q}\sqrt{\frac{1-\omega_q}{1+\omega_q}} \\ \left(\frac{1}{\alpha}\sqrt{\frac{2p_1\Lambda_A(\gamma_0 z_q+1)}{\lambda_0 K_1(1-\nu_1)\gamma_0}}\right)^{q_1+\frac{1}{2}}\mathcal{K}_{q_1+\frac{1}{2}}\left(\frac{1}{\alpha}\sqrt{\frac{2p_1\Lambda_A(\gamma_0 z_q+1)}{\lambda_0 K_1(1-\nu_1)\gamma_0}}\right) \\ \left(\frac{1}{\beta}\sqrt{\frac{2p_2 z_q}{\lambda_0 K_2(1-\nu_2)}}\right)^{q_2+\frac{3}{2}}\mathcal{K}_{q_2-\frac{1}{2}}\left(\frac{1}{\beta}\sqrt{\frac{2p_2 z_q}{\lambda_0 K_2(1-\nu_2)}}\right), \end{aligned} \tag{B-3}$$

where $z_q = -\ln\frac{(\omega_q+1)a}{2}$, $a = \exp\left(-\frac{\Lambda_B}{\gamma_0}\right)$, $\omega_q = \cos\left(\frac{2q-1}{2Q}\pi\right)$, and Q is the complexity-vs-accuracy trade-off coefficient. By substituting (B-3) into (B-1), the proof is completed.

References

1. Tran, D.D., Tran, H.V., Ha, D.B., Kaddoum, G.: Secure transmit antenna selection protocol for MIMO NOMA networks over Nakagami-m channels. IEEE Syst. J. **14**(1), 253–264 (2020)
2. Liu, Q., Sun, S., Yuan, X., Zhang, Y.: (2021) Ambient backscatter communication-based smart 5G IoT network. EURASIP J. Wirel. Commun. Netw. **1**, 1–19 (2021)

3. Zhou, F., Wu, Y., Hu, R.Q., Qian, Y.: Computation rate maximization in UAV-enabled wireless powered mobile-edge computing systems. IEEE J. Sel. Areas Commun. **36**(9), 1927–1941 (2018)
4. Dogra, A., Jha, R.K., Jain, S.: A survey on beyond 5G network with the advent of 6G: architecture and emerging technologies. IEEE Access **9**, 67512–67547 (2021)
5. Chen, Z., Ma, X., Han, C., Wen, Q.: Towards intelligent reflecting surface empowered 6G terahertz communications: A surv. China Communications. **18**(5), 93–119 (2021). https://doi.org/10.23919/JCC.2021.05.007
6. Akbar, A., Sobia Jangsher, F.A.B.: NOMA and 5G emerging technologies: a survey on issues and solution techniques. Comput. Netw. **190**, 107950 (2021). https://doi.org/10.1016/j.comnet.2021.107950
7. Pereira De Figueiredo, F.: An overview of massive MIMO for 5G and 6G. IEEE Lat. Am. Trans. **20**, 931–940 (2022). https://doi.org/10.1109/TLA.2022.9757375
8. Hou, T., Liu, Y., Song, Z., Sun, X., Chen, Y.: Multiple antenna aided NOMA in UAV networks: a stochastic geometry approach. IEEE Trans. Commun. **67**(2), 1031–1044 (2019)
9. Hou, T., Liu, Y., Song, Z., Sun, X., Chen, Y., Hanzo, L.: Reconfigurable intelligent surface aided NOMA networks. IEEE J. Sel. Areas Commun. **38**(11), 2575–2588 (2020). https://doi.org/10.1109/JSAC.2020.3007039
10. Alghamdi, R.: Intelligent surfaces for 6g wireless networks: a survey of optimization and performance analysis techniques. IEEE Access **8**, 202795–20281 (2020). https://doi.org/10.1109/ACCESS.2020.3031959
11. Do, D.T., Nguyen, T.L., Lee, B.M.: Performance analysis of cognitive relay-assisted ambient backscatter with MRC over Nakagami-m fading channels. Sensors **20**(12), 3447 (2020). https://doi.org/10.3390/s20123447
12. Al-Eryani, Y., Hossain, E.: The D-OMA method for massive multiple access in 6G: performance, security, and challenges. IEEE Veh. Technol. Mag. **14**(3), 92–99 (2019). https://doi.org/10.1109/MVT.2019.2919279
13. Khalid, W., Kaleem, Z., Ullah, R., Chien, T., Noh, S., Yu, H.: Simultaneous transmitting and reflecting-reconfigurable intelligent surface in 6G: design guidelines and future perspectives. IEEE Netw. https://doi.org/10.1109/MNET.129.2200389
14. Aldababsa, M., Khaleel, A., Basar, E.: STAR-RIS-NOMA networks: an error performance perspective. IEEE Commun. Lett. **26**(8), 1784–1788 (2022)
15. Wu, C., Mu, X., Liu, Y., Gu, X., Wang, X.: Resource allocation in STAR-RIS-aided networks: OMA and NOMA. IEEE Trans. Wireless Commun. **21**(9), 7653–7667 (2022)
16. Zuo, J., Liu, Y., Ding, Z., Song, L., Poor, H.V.: Joint design for simultaneously transmitting and reflecting (STAR) RIS assisted NOMA systems. IEEE Trans. Wireless Commun. **22**(1), 611–626 (2022)
17. Zheng, C., Zhou, W.: Computation bits maximization in backscatter-assisted wireless-powered NOMA-MEC networks. EURASIP J. Wirel. Commun. Netw. **2022**(1), 23 (2022). https://doi.org/10.1186/s13638-022-02097-4
18. Zargari, S., Tellambura, C., Herath, S.: Energy-efficient hybrid offloading for backscatter-assisted wirelessly powered MEC with reconfigurable intelligent surfaces. IEEE Trans. Mob. Comput. **22**(9), 5262–5279 (2023). https://doi.org/10.1109/TMC.2022.3177454
19. Ding, Z., Fan, P., Poor, H.V.: Impact of non-orthogonal multiple access on the offloading of mobile edge computing. IEEE Trans. Commun. **67**(1), 375–390 (2019)
20. Gong, S., Xie, Y., Xu, J., Niyato, D., Liang, Y.C.: Deep reinforcement learning for backscatter-aided data offloading in mobile edge computing. IEEE Netw. **34**(5), 106–11 (2020). https://doi.org/10.1109/MNET.001.1900561

21. Shi, L., Ye, Y., Chu, X., Lu, G.: Computation bits maximization in a backscatter assisted wirelessly powered MEC network. IEEE Commun. Lett. **25**(2), 528–532 (2021). https://doi.org/10.1109/LCOMM.2020.3027294
22. Cheng, Y., Li, K.H., Liu, Y., Teh, K.C., Vincent Poor, H.: Downlink and uplink intelligent reflecting surface aided networks: NOMA and OMA. IEEE Trans. Wirel. Commun. **20**(6) (2021). https://doi.org/10.1109/twc.2021.3054841, URL http://dx.doi.org/10.1109/TWC.2021.3054841
23. Ye, Y., Lu, G., Hu, R.Q., Shi, L.: On the performance and optimization for MEC networks using uplink NOMA. In: IEEE International Conference on Communications Workshops (ICC Workshops), Shanghai, China, pp. 1–6 (IEEE) (2019)
24. Truong, V.T., Ha, D.B., Vu, T.T., Nguyen, H.A.: STAR-RIS aided mobile edge computing networks with uplink NOMA scheme. In: 2023 International Conference on Advanced Technologies for Communications (ATC), pp. 474–479 (Da Nang, Vietnam) (2023)
25. Gradshteyn, I., Ryzhik, I.: Table of Integrals, Series, and Products, Elsevier Academic Press (2007)